Journal of Alloys and Compounds 947, (2023), 169521
https://doi.org/10.1016/j.jallcom.2023.169521
Accepted 3 March 2023

Melt/solid interaction and melt super-saturation effect on the microstructure asset of ultra-refractory composites prepared by reactive melting infiltration

Laura Silvestroni[1*], Antonio Vinci[1], Nicola Gilli[2], Luca Zoli[1], Diletta Sciti[1], Dietmar Koch[3], Marius Kütemeyer[4]

[1]*CNR-ISSMC (former ISTEC), Institute of Science, Technology and Sustainability for Ceramics, Via Granarolo 64, 48018 Faenza, Italy*

[2]*CNR-IMM, Institute for Microelectronics and Microsystems, Via Gobetti 101, 40129 Bologna, Italy*

[3]*Univ. of Augsburg, Inst. of Mater. Resource Management, Am Technologiezentrum 8, 86159 Augsburg, Germany*

[4]*German Aerosp. Center (DLR), Inst. of Struct. and Design, Pfaffenwaldring 38-40, Stuttgart 70569, Germany*

Abstract

The reactions occurring between a Zr_2Cu melting phase and possible compounds intended for use in ultra-refractory ceramic matrix composite, i.e. SiC, TiB_2 and ZrB_2 are first explored through sessile drop tests, confirming a promising infiltration capability of the melt. Then, a multiphasic ultra-high temperature ceramic matrix composite was prepared by reactive melt infiltration (RMI), using a TiB_2-coated carbon fiber preform infiltrated with Zr_2Cu at 1500°C which resulted in the precipitation of ZrB_2 and ZrC sub-micrometric faceted grains and a general damage of both fiber and fiber coating, which were penetrated by the melt. Then, to decrease the RMI process temperature down to 1200°C and limit the fiber damage degree, a second composite was prepared introducing an additional ZrB_2-B infiltration step. Although processing at 300°C lower, notable alteration of the fiber occurred upon reaction with the Zr_2Cu melt and developed a ZrC scale around them, but still allowing pull-out. In addition, the local B-rich environment promoted the development of a dual-phase microstructure within the matrix composed of new sub-micrometric grains and of larger ZrB_2 grains, partially dissolved in the melt and re-precipitated acquiring a nano-sized lamellar eutectic structure. The combination of factors on multiple scale length, from the micro- of the fiber to the nano-of the lamella, seems to provide synergistic reinforcing phenomena and thus could be a valuable approach to develop materials for extreme environments.

Keywords: Borides; reaction melt infiltration; dual-phase microstructure; eutectic structure.

1. Introduction

With the advancement of new aerospace vehicle designs, sharp components are essential to enable better maneuverability and higher performance. Significant aerodynamic drag, and hence localized

* Corresponding author: Laura Silvestroni
Tel. +39 546 699723
Fax. +39 546 46381
e-mail. laura.silvestroni@istec.cnr.it

aerodynamic heating, characterizes the sharpest components of these vehicles, which are thus the most solicited regions. As such, they require a combination of thermo-mechanical properties which are currently unmet by currently used materials. Failure tolerance, resistance to thermal shock, high temperature stability in oxidizing environment are some of the key properties which have to be simultaneously achieved in new generation materials to sustain hypersonic flights. Current C_f/C and C_f/SiC composites, although they might be suitable for very short flight durations, are not appropriate for an extended flight envelope [1], [2]. Indeed, acute tips will touch temperature above 2000°C and, in oxidizing environment, both types of composites will suffer remarkable ablation [3], [4]. Promising materials to be used at such temperature with minimal erosion are the class known as ultra-high temperature ceramics (UHTCs),[5] which possess melting points over 3000°C and have zirconium diboride (ZrB_2) as forefather [6], [7]. The union between the classical ceramic matrix composites (CMCs) and UHTCs has recently generated a new class of hybrid materials, named UHTCMCs, having a refractory ceramic as matrix, and SiC or C fibers as reinforcement [8]–[14]. Tailoring the matrix chemistry and morphology on one side and the amount and type of reinforcement on the other side promise unprecedented performances in extreme environment, by combining the strengths of both components.

Reactive melt infiltration (RMI) is a convenient technique to produce ceramic matrix composites [15]–[19]. It is advantageous over other fabrication techniques, like polymer infiltration and pyrolysis (PIP) or chemical vapor infiltration (CVI), in terms of shorter producing times, lower costs, lower fraction of residual porosity and possibility to obtain large parts and near-net-shape components [20]. The process utilizes porous preforms, which are infiltrated by a melt that, under the driving force of capillary action, fills the pores, reacts with the preform and ultimately yields a dense composite with a matrix dependent on the chemistry of the melt, the features of the preform and the infiltration atmosphere used. However, as main drawbacks, the RMI method uses melts which can be very aggressive towards the fiber, like the case of transition metals containing ones, so a protective coating is often required. Furthermore, the final density of the component might be relatively high, owing to residual metal alloy or new reaction products trapped in the matrix.

The most commonly employed melt is silicon which results in high performance C_f/C-SiC composites [21]. Despite the complexity and dynamicity of the RMI process, subject to element concentration and temperature local variations, recent literature reported good agreement between modelling of channel filling and reaction phase formation with experimental data in Zr-Si-C systems,[22], [23] putting forward the practicability of a more controllable process even in more complex system as compared to the conventional Si-C one.

In the perspective of increasing the high temperature stability of composites, the wetting behavior of the melt towards the porous C_f/UHTC preform is fundamental for the success of the RMI process. Therefore, the most important parameters for achieving a suitable infiltration depth during the process are:

- atmosphere and infiltration temperature, which in turn impacts on
- melt viscosity and contact angle with the preform,
- reaction phases and corresponding properties,

The ideal phase should have a low melting temperature to enable easy processing, it should homogeneously wet the preform and react or decompose forming high melting point compounds.

Possible candidates to obtain a ZrB_2-filled carbon fiber fabric include copper, silicon or Zr-Cu alloys. Si melts at higher temperature, 1400°C, wets ZrB_2, but the reaction products are Zr_xSi_y which have low melting phases and are brittle.[24] In addition, the volume expansion due to SiC formation needs higher infiltration temperatures necessary. Amongst Zr-Cu alloys, Zr_2Cu has a low congruent temperature at 1025°C.

Copper melts at 1085°C and Zr-Cu alloys are liquid already from about 900°C.[25] The Zr released by the liquid Zr_2Cu is very reactive and can form additional ZrB_2, in the presence of boron sources (R1), or ZrC, upon reaction with the fibers (R2).

$Zr_2Cu + 4B \rightarrow 2ZrB_2 + Cu$ R1

$Zr_2Cu + 2C \rightarrow 2ZrC + Cu$ R2

Thermodynamics calculations revealed that reaction R1 could occur at temperatures as low as 1100°C.[26] As the melt gets impoverished of Zr, the stoichiometry changes and the alloy becomes increasingly richer in copper, which does not wet ZrB_2 properly as featured by a contact angle >120°[27] and no interaction [28] and is also associated to a volume increase resulting from reaction R1, which pushes the residual Cu-alloy to segregate to the surface.

Besides the melt/UHTC matrix interactions, the melt/fiber reaction must also to be taken into account. Unfortunately, like all compounds containing metals, Zr_2Cu strongly reacts with carbon fiber and would convert it to polycrystalline ZrC, thus losing the carbon fiber reinforcing effect. Typical coating for carbon fibers are pyrolytic carbon, which would just delay but not block the consumption process, or better SiC or TiB_2, in view of their compatibility with the ZrB_2 matrix and envisaged working environment.[28] The information regarding the interaction between the selected melt, Zr_2Cu, and the possible coatings, SiC or TiB_2, has been poorly investigated, but it is of fundamental importance for defining the fracture behavior of the final composite, i.e. a low reactivity would guarantee fiber integrity, the desired fiber pull-out and UHTC toughening.[29], [30] Studying the wetting behavior between melts and SiC substrate is important also in view of extending the findings to polycarbosilane, which could be used as infiltration medium.

The goals of this study are multiple:

1) to check the interaction between a Zr_2Cu melt and possible fiber coating, i.e. SiC, TiB_2, ZrB_2;

2) to assess the reliability of sessile drop tests as fast method for evaluating the actual behavior of a UHTCMC produced by reactive melt infiltration;

3) to use a low temperature melting and low viscosity phase as reactive compound to improve the infiltration within a C preform, to avoid the need of a fiber coating, and to neutralize residual Cu-based low melting

phases by dissolution and formation of more refractory compounds, i.e. to produce further ZrB_2 upon the infiltration process.

Under these perspectives, the sessile drop technique is here used to understand the interactions between the reactive melt and the three substrates; subsequently, infiltration of a porous TiB_2-coated carbon fiber preform composite by Zr_2Cu was accomplished, and then additional boron was introduced to the system to prepare a second composite using naked carbon fibers.

The resulting diffusion couples and UHTC composites were investigated from a microstructural point of view to highlight key process parameters for optimizing the RMI process of UHTCMCs.

2. Experimental procedure

2.1 Materials

To investigate the interaction between melt and ZrB_2, TiB_2 or SiC, the following fully dense ceramics were used as substrates: a fully dense ZrB_2 ceramic provided by CNR-ISSMC (former ISTEC), Italy and produced according to the procedure described in [31], fully dense SiC and TiB_2, both provided by FCT Ingenieurkeramik GmbH, Germany. As melting phase, Zr_2Cu was used (HMW Hauner GmbH & Co. KG). The substrate materials were cut into 15 mm X 15 mm square plates with thicknesses between 2-3 mm and polished using diamond suspensions on a range of polishing discs, with an average surface roughness of 0.1 µm. Before beginning the wetting experiments, the polished surfaces were cleaned using ethanol and acetone and then rinsed in an ultrasonic bath.

Subsequently, a UHTCMC was produced by RMI using Zr_2Cu as melting phase as described in [15], essentially comprising the following steps: deposition of TiB_2 by chemical vapor deposition (CVD) on pitch-based carbon fibers sheets (XN80 Granoc, Nippon Graphite Corporation), infiltration of the TiB_2 coated preform with a polycarbosilane (Starfire SMP-877) enriched with 70 wt% amorphous B powder (Tradium GmbH 95/97); stacking of the coated sheets in 0/90° configuration, dry, cure and pyrolysis and reactive infiltration with the Zr_2Cu melting phase at 1500°C. This material was labeled as 1. The size of the composite was 50x50 mm^2 with a thickness of about 10 mm and the penetration height was about 41 mm, as reported in [15].

Active phases, like B and C, can be used to further decrease the amount of residual melt inside the UHTCMC matrix.[28], [30] Therefore, in a following test, with the aim of preserving the fiber integrity and skipping the expensive and time consuming CVD process to deposit the TiB_2 coating, a 1 at% B-modified Zr_2Cu alloy (HMW Hauner GmbH & Co. KG) was selected to decrease the viscosity of the melting phase (from 10^3 to $8x10^4$ MPa·s at 1320°C) and better infiltrate the carbon fiber preform.[28] In addition, to decrease the unreacted Zr-Cu residuals, a ZrB_2-25 vol% B slurry was used as infiltration UHTC source prior to the reactive stage.[32] For this material, labeled as 2, the procedure consisted in the infiltration of unidirectional fiber preforms with the ZrB_2-B slurry and subsequent reaction with the Zr_2Cu-B melt bath at 1200°C. Also in this

case, the size was 50x50 mm^2 with 8 mm height, but differently from sample 1, it was fully infiltrated, including the sample holder.[32]

2.2 Wetting tests

Using the DSAHT LORA 1700 contact angle measurement system (KRUESS), a small granule of Zr_2Cu alloy was placed atop the flat ceramic plate and heated from room temperature in the small tube furnace at ambient pressure under an Ar atmosphere. The furnace controller was set at a heating rate of 10 K/min from 25-1000°C, 7 K/min from 1000-1200°C and 5 K/min between 1200-1500°C, with a total experimentation cycle ranging within 8-10 hours. The peak temperature for each experiment, 1500°C, was held for 20 minutes before controlled cooling at a rate of 5K/min. Between 1000-1200°C the melting temperature of all sample alloys was reached and some form of wetting was observed. Using windows fitted at the end of the furnace, the DSA4 camera system took drop-shape images of the melt's shadow and recorded the associated contact angle; taking 4-5 images/K. Contact angles were recorded at 50°C intervals at the triple line points, at both the left and right sides of the droplet. The DSA4 software measures the volume and surface area of the drop as it wets, fitting the silhouette to Young-Laplace or Tangent algorithms and providing information about the melt's spreading behavior.

2.3 Characterization

The microstructure upon substrate/drop interaction and cross section of the UHTCMCs was analyzed on polished cross-sections by field-emission scanning electron microscopy (FESEM, mod. ΣIGMA, ZEISS NTS Gmbh, Germany) coupled to an energy dispersive X-ray micro-analyzer (EDS, mod. INCA Energy 300, Oxford Instruments, UK). For a selected material, a specimen was prepared for analysis by transmission electron microscopy (TEM, FEI Tecnai F20 ST) by conventional mechanical grinding. Local phase analysis was performed with an acceleration voltage of 200 kV. The TEM was equipped with an EDAX EDS X-ray spectrometer PV9761 with a super ultra-thin window. Indexing of diffraction patterns was carried out through the commercial software JEMS (Java Electron Microscopy Software, P. Stadelmann, Switzerland).

3. Results and Discussion

3.1 Contact Angle Measurements

Table I summarizes the contact angles measured at 1200 and 1500°C on several substrates using different melt phases. Zr_2Cu starts melting at around 1020°C, wetting the SiC substrate at an angle of 56°. Small decreasing steps in the contact angle (25°) could be measured at 1026°C, and again (15°) at 1057°C. By 1065°C the melt fully wetted the SiC substrate. Both ZrB_2 and TiB_2 experienced very low contact angles, less than 10°, shortly after melting. The Zr_2Cu alloy hence proved to display sufficient wetting tendency to promote infiltration of either SiC or Zr/TiB_2-based substrates.

Given the lower viscosity of the B-modified Zr_2Cu alloy, also this compound showed to be suitable for the reactive melt infiltration process.

Table I: Summary of the contact angles at 1200 and 1500°C on SiC, ZrB_2 and TiB_2 using Zr_2Cu and B-doped Zr_2Cu as melting phases.[29]

Substrate	***Melt***	***Contact Angle [°]***	
		1200°C	*1500°C*
SiC	*Zr_2Cu*	*65*	*<10*
	Zr_2Cu-1B	*45*	*<10*
TiB_2	*Zr_2Cu*	*<10*	*<10*
	Zr_2Cu-1B	*<10*	*<10*
ZrB_2	*Zr_2Cu*	*<10*	*<10*
	Zr_2Cu-1B	*n.a.*	*n.a.*

3.2 Microstructure analysis

3.2.1 Sessile drop tests

Substrates

The three ceramic substrates, SiC, TiB_2 and ZrB_2 were characterized by negligible residual porosity as ascertained by SEM inspection. SiC matrix contained less than 10 vol% B_4C particulates and TiB_2 impurities; TiB_2 had a fraction of nitride impurities below 3 vol% and ZrB_2 contained minor amounts of secondary phases including SiC, ZrO_2, $ZrSi_2$ and SiO_2-based species, altogether below 5 vol%.

SiC-Zr_2Cu system - The interaction between the Zr_2Cu alloy and the SiC substrate was very poor, although the drop had enough wettability. Indeed, the drop detached from the ceramic phase without development of any reaction phase, Fig. 1a. The microstructure of the unaltered substrate and drop are illustrated in Fig. 1b,c, respectively.

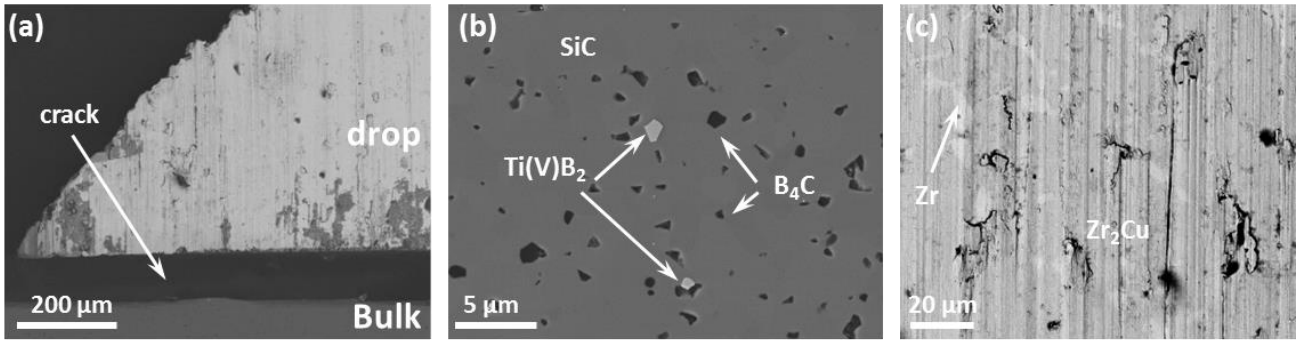

Fig. 1: SEM images of the cross section upon wetting between SiC/Zr_2Cu at 1500°C. a) Overall view of the detached drop, b) magnification of the unaltered SiC bulk substrate and c) of the alloy drop.

TiB_2-Zr_2Cu system - The Zr_2Cu alloy showed good wettability towards the TiB_2 substrate too, but tensional stresses developed and provoked cracks at the ceramic side. Analysis of the cross section in Fig. 2a revealed

that reactions mostly occurred in the melt rather than in the ceramic, which remained apparently unaltered. Just at the interface, Zr-C based phases formed at the TiB_2 grain boundaries, as evidenced in the inset of Fig. 2a. The melt composition can be divided in two regions, in the upper part of the drop, labeled as I in Fig. 2b and magnified in Fig. 2c-e, flower-like features developed within the Zr_2Cu phase, as a consequence of its dissociation already at low temperature. These were biphasic structures with Zr-C and ZrB_2 as major components. Moving toward the TiB_2 ceramic, labeled as II in Fig. 2b and magnified in Fig. 2f,g, the ceramic was mostly composed of the Zr_2Cu matrix where new ZrB_2 tiny grains precipitated. ZrB_2 became progressively more abundant and fine at the interface with TiB_2, Fig. 2f. Possible reactions leading to formation of ZrB_2 phase are proposed in R3-R5:

$$4TiB_2 + Zr_2Cu \rightarrow 2ZrB_2 + Cu + 4TiB \quad (R3)$$

$$2TiB_2 + 3Zr_2Cu \rightarrow 3ZrCu + ZrTi_2 + 2ZrB_2 \quad (R4)$$

$$2TiB_2 + Zr_2Cu + 2C \rightarrow 2ZrB_2 + Cu + 2TiC \quad (R5)$$

The Zr_2Cu phase is not present in most common thermodynamic databases, so it is difficult to assess which of the above reactions is the most favorable. Most thermodynamic calculations treat Zr_2Cu as a mixture of its individual constituents, Zr and Cu, and therefore any calculated ΔG of reaction would account only for the reaction between Zr and the reactant, either B or C. However, given the reducing environment and the ease of formation of TiC over TiB, reaction R5 is the most probable to occur.

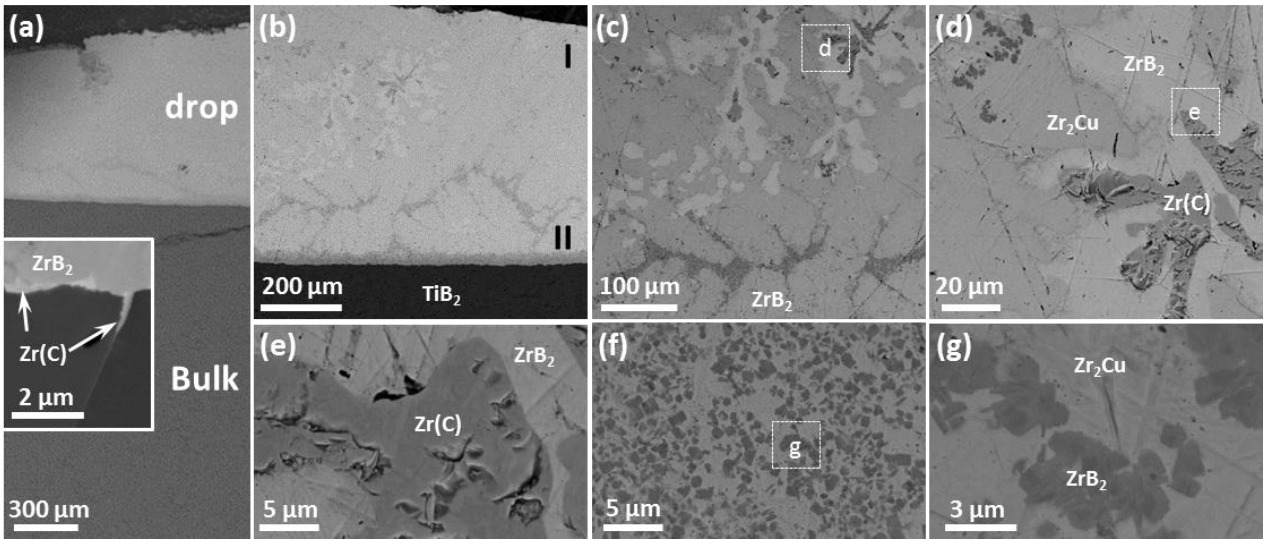

Fig. 2: SEM images of the cross section upon wetting between TiB_2/Zr_2Cu at 1500°C. a) Overall view with inset a detail of the drop/substrate interface, b) magnification of the drop, c) layer I, d)- e) detailed views of the flower-like microstructure in I, f)-g) layer II.

ZrB_2-Zr_2Cu - The Zr_2Cu drop, after reaching 1500°C, was well adherent to the ZrB_2 substrate. A cross section image of the joint is shown in Fig. 3a and a complex architecture can be recognized: two distinct regions, layer I and II, composed the Zr_2Cu drop, while the substrate was comprised by a reaction zone, layer III and the bulk ceramic itself. Starting from the top, a bright region composed of Zr/Zr_2Cu was the residual of the melt containing also complex metal silicides, Fig. 3b. Then, a 340 µm thick layer mostly based on $ZrB_2/Zr/Zr_2Cu$

and Zr-Cu-Si alloys followed, Fig. 3c,d. Entering into the ceramic substrate, a 770 µm thick Si-depleted region was observed, Fig. 3f, before entering the unreacted bulk material, Fig. 3g. All the interfaces between these four regions were coherent and smooth, Fig. 3e, indicating a good solubility of the constituting elements and the strong tendency of Si-based phases, present in the as sintered ceramic, to be drained by capillary forces and react with the Zr_2Cu melt. This sequence of layers may indicate either a higher tendency of Zr_2Cu to dissociate in presence of Si-species, as compared to a cleaner system observed in the case of TiB_2 substrate, or suggests that the ceramic matrix significantly dissolved in the melt, probably promoted by the silicide phases abundance in layer II, and was drained from the bulk material.

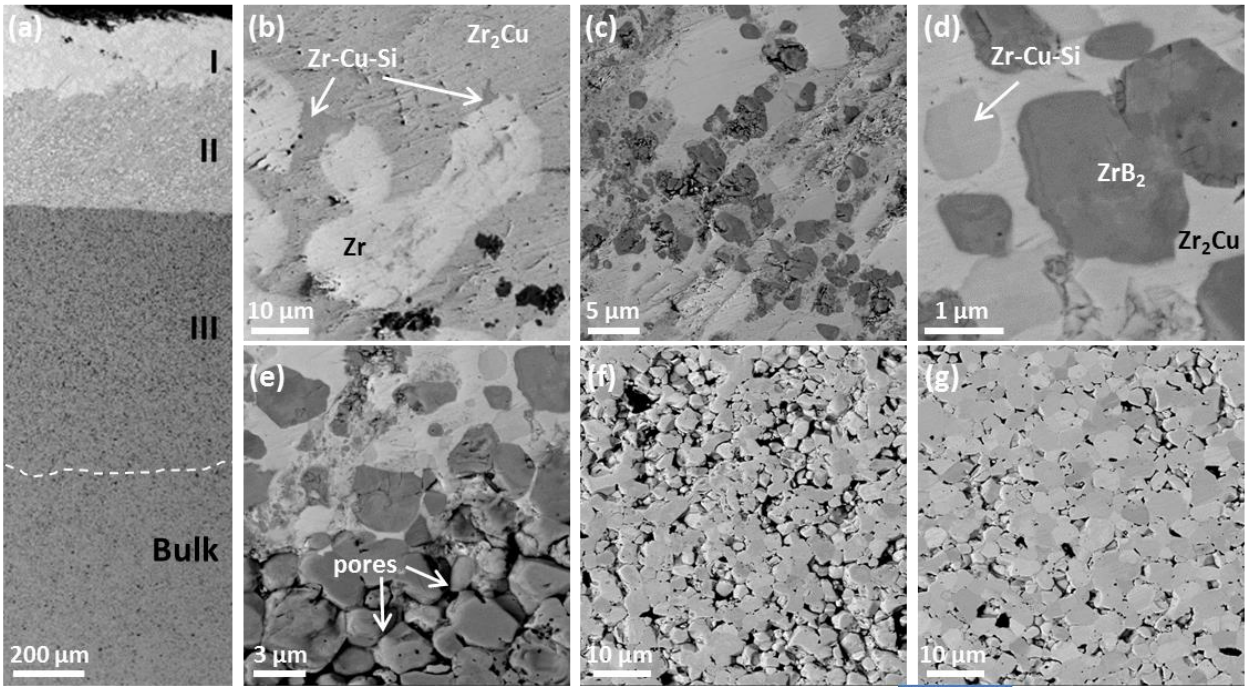

Fig. 3: SEM images of the cross section upon wetting between ZrB_2/Zr_2Cu at 1500°C. a) Overall view and b) magnification of layer I, c) of layer II, d) detailed view of the microstructure in II, e) interface between layer II and III, f) layer III and g) unaltered bulk substrate.

Overall, these tests evidenced that moving from SiC to TiB_2 to ZrB_2, an increase in reactivity occurred with the Zr_2Cu melt, putting forward the need to cover the carbon fiber with either a SiC or TiB_2 layer to preserve its reinforcing action in a UHTC composite.

3.2.2 TiB_2-coated UHTCMC with Zr_2Cu melt (Material 1)

The microstructure of the TiB_2-coated UHTCMC composite is shown in Fig. 4. The external surface was covered with Cu, which is an expected behavior owing to reaction of the alloy with the composite itself. In a user-perspective, the surface should be in any case scraped to remove such low-melting metal. Low magnification images show a very good infiltration level and no major porosity across the thickness, but just scattered in fiber-rich zones, Fig. 4a. The distance between two subsequent fiber layers was rather homogeneous and averaged 150 µm, Fig. 4b. Occasionally, cracks were observed to depart from the fiber

and to cross the UHTC region. In a future material optimization step, the distance between subsequent fiber layers could be decreased to simultaneously minimize tensile stresses rising in the dense matrix and increase the fiber volume fraction, thus reducing the overall density of the composite. Cracks are indeed commonly found if the matrix to fiber ratio is unbalanced during stacking, or there are inhomogeneous zones, due to the thermo-elastic properties mismatch between the carbon fiber and the UHTC matrix. In the area between the UHTC-rich matrix and each fabric layer, progressive TiB_2 coating consumption was observed consistently, Fig. 4c, in agreement with the wetting tests that showed formation of new ZrB_2 grains at the interface between the metal alloy and TiB_2, Fig. 2f,g.

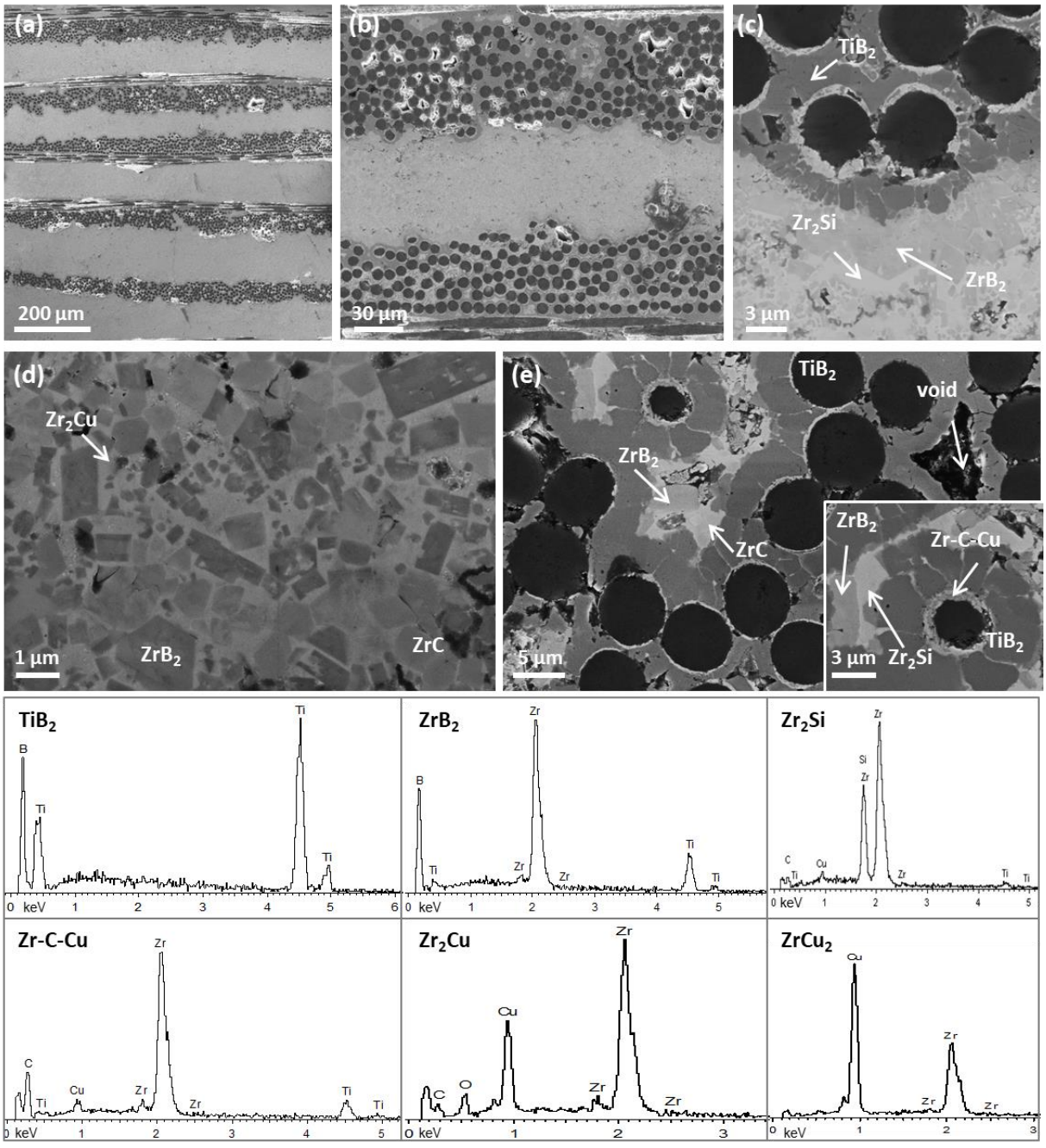

Fig. 4: SEM images of the cross section of the TiB_2-coated Cf preform infiltrated with Zr_2Cu alloy, material 1. a) Overall view, b) magnification of the fiber/matrix asset and detailed view of c) fiber/matrix interface, d) matrix, e) fiber boundle multiphase structure with EDS of the corresponding phases below.

A closer inspection on the UHTC matrix revealed a very complex but homogeneous microstructure characterized by faceted squared ZrB_2 and ZrC tiny grains immersed into a Zr_2Cu matrix, Fig. 4d. The composition of the grains varied and solid solutions including Ti into Zr-boride and carbide lattices were often found, especially in proximity of fiber-rich areas, since TiB_2 was covering the fiber. In these zones, around the carbon fiber, the TiB_2 coating was well visible as discontinuous dark grey layer, about 1-3 µm thick, Fig. 4b. Cracking of the TiB_2 coating is in agreement with the cracking observed upon the sessile drop test, Fig. 2a, and possibly due to the large coefficient of thermal expansion mismatch between the boride and the metal alloy.[7], [33] As a consequence of the discontinuous TiB_2 coating, at the C/TiB_2 interface, all fibers developed a 500 nm thin bright interlayer based on (Zr,Ti,Cu)C, Fig. 4c. The bright phase within the fiber bundle was again a mixture of ZrB_2, ZrC, $ZrSi_2$ and Zr_xCu_y. The silicide phase derives from the infiltration with the polycarbosilane.

The microstructure analysis of material 1 demonstrated that sessile drop tests reproduced in a rather accurate way the behavior of the reactive melting environment and demonstrated that the interactions occurring in such complex UHTCMC system can be split and understood in simple separate wetting tests. In addition, material 1 pointed to the fact that a fiber coating, if not well coherent and continuous, does not offer sufficient protection to the corrosive action of the penetrating melt. Therefore, the design concept behind the next composite included the use of an uncoated fiber preform and a ceramic matrix containing extra elemental boron, to promote the preferential in-situ formation of ZrB_2 instead of ZrC. From thermodynamic simulations, the formation of ZrB_2 from the elemental constituents is more thermodynamically favored as compared to the formation of ZrC in the temperature range investigated, Fig. 5. Therefore, the presence of elemental boron can effectively limit the fibre degradation and simultaneously lead to the formation of an UHTC phase in the material, namely ZrB_2. However, due to the high affinity of B with Zr, the reaction is difficult to control and can quickly create a barrier towards further diffusion of the melt within the matrix, by halting the infiltration process. In order to limit this phenomenon, raw ZrB_2 powders in varying ratios were added as filler in the boron powder suspensions, as presented in a previous study.[32] In the following material of the present work, the B-to-Zr vol% was 25-to-75%.

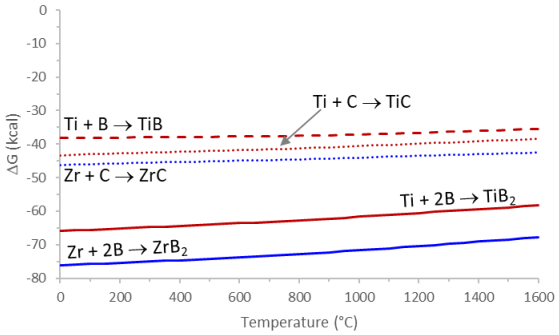

Fig. 5. Gibbs free energy variation calculated at 1 bar for the formation of carbides and borides of Ti and Zr starting from the elemental constituents.

3.2.3 ZrB_2-B impregnated UHTCMC with Zr_2Cu melt (Material 2)

The microstructure and properties of this composite had been presented in a previous study,[32] but for the sake of clarity the main microstructural features will be summarized, together with additional TEM analysis. Despite the relatively low processing temperature, the carbon fiber notably reacted with the surrounding Zr_2Cu melt leading to the formation of ZrC at the interface, Fig. 6a, which formed a sort of rim around the fiber with grains of progressively coarser size, according to reaction R1. However, the combined presence of boron and carbon, within a reducing environment, could trigger a multi-step formation pathway according to reactions R6-R8:

$Zr_2Cu + 2B + C \rightarrow ZrB_2 + ZrC + Cu$ R6

$ZrB_2 + C \rightarrow ZrC + 2B$ R7

$ZrB_2 + CO + 1/2O_2 \rightarrow ZrC + 2B_2O_3$ R8

R7 is not thermodynamically favorable in the temperature range investigated ($\Delta G > 0$), but R8 is.

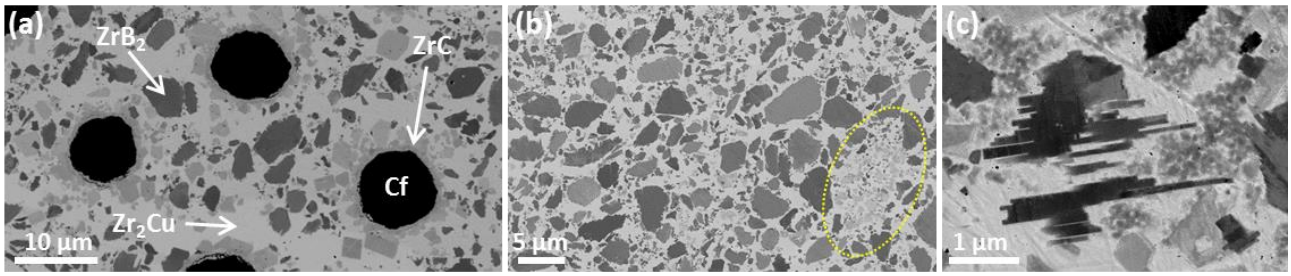

Fig. 6: SEM images of the cross section of the ZrB_2-B impregnated and reaction melt infiltrated UHTCMC, material 2. a) Overall view of the fiber/matrix asset, b) magnification of the matrix highlighting nano-sized ZrB_2 grains beside the micron-sized ones and c) detailed view of a corroded ZrB_2 grain showing lamellar eutectic structures.

Beyond the ZrC layer around the fibre, two types of ZrB_2 grains were identified: 100-300 nm small ones, deriving from the reaction between boron present in the slurry and the Zr_2Cu phase, and 2-3 µm wide ones, deriving from the ZrB_2-B-based slurry impregnation before the reactive melting step, Fig. 6b. The first group of grains had faceted boundaries and squared shape, as typically found in metal-rich cermets and other crystals deriving from reactive processes.[34]–[36] These sub-micron sized ZrB_2 grains were immersed into residual Zr-Cu alloy, where CuO phase was often found at the grain boundaries and recognizable as black smears, Fig. 7b,c. In turn, within this trapped oxide phase, Cu precipitates were found as illustrated in the EDS profile in Fig. 7d. As for the second group of grains, i.e. the larger ones, reminiscent of the original ZrB_2 powder composing the slurry, were featured by edge consumption in a peculiar way, Fig. 6c, and by the systematic presence of dislocation network at the boride/alloy interface, Fig. 7e, owing to the large thermo-elastic constant mismatch between the boride and the metal alloy.[37]

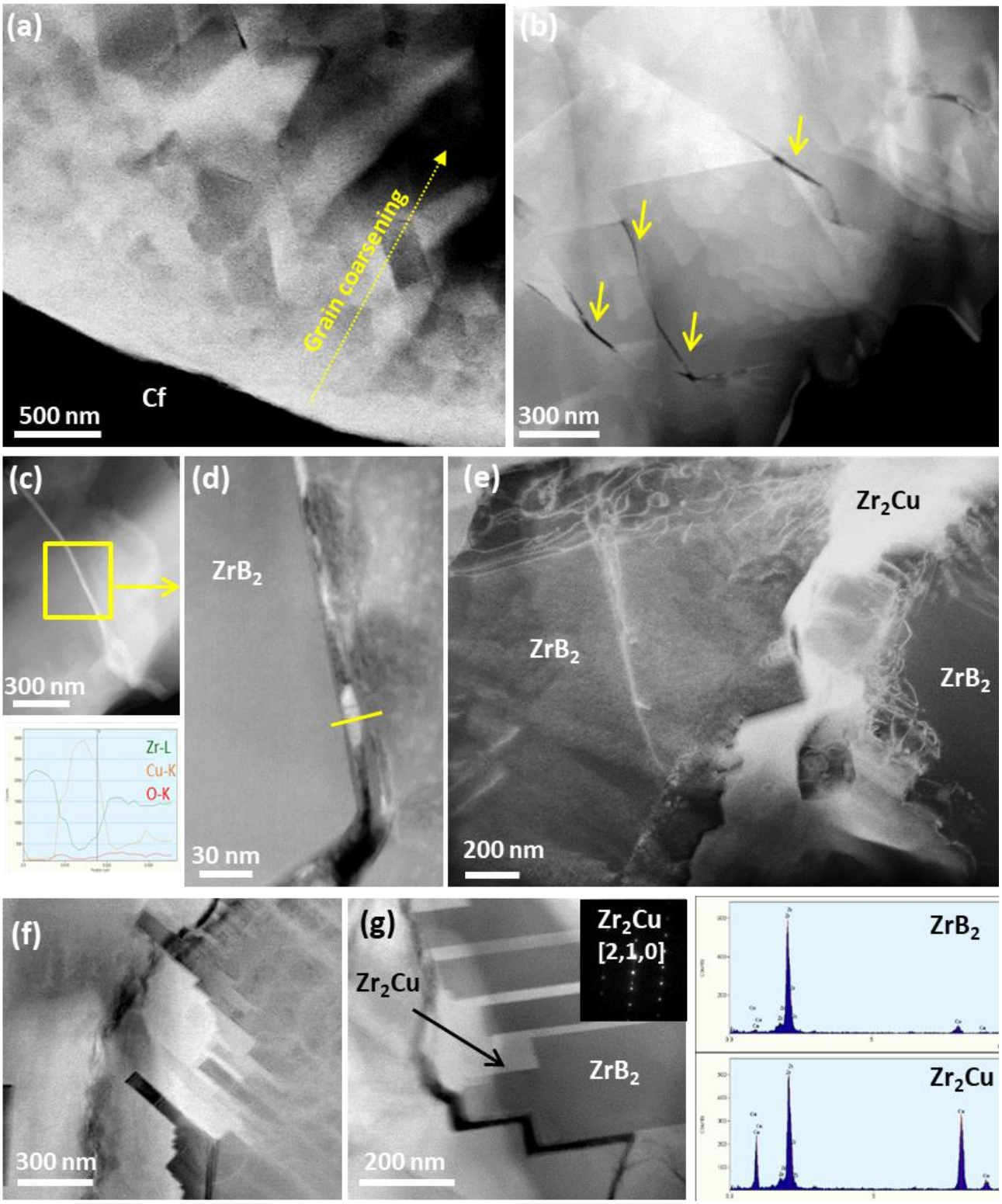

Figure 7. TEM images of the RMI UHTCM, material 2, showing a) progressive grain coarsening moving from the fiber to the matrix, b) CuO black smears trapped at the ZrB_2/Zr_2Cu grain boundaries pointed by arrows with c) & d) EDS profile spectra with magnification of Cu precipitates within the oxide. e) Dislocations within ZrB_2 grains adjacent to the Zr_2Cu melt, f) & g) examples of lamellar eutectic structures with EDS of the dark (ZrB_2) and bright (Zr_2Cu) laths.

Each large ZrB_2 grain was partially dissolved in the melting Zr_2Cu phase and, upon cooling, developed a lamellar-like boundary where laths of ZrB_2 were alternating laths of Zr_2Cu, Fig. 7f,g, as typically observed during the crystallization of a metallic alloy from a mixture of eutectic composition.[38] Cu-oxide phases were systematically found also at the apical terminations of these lamellar structures were dark contrasted linear features delineated a precipitation front between crystalline ZrB_2 and the newly formed ZrB_2 nano-sized grains precipitating from the melt, Fig. 8a,b, suggesting poor wettability between the oxide and the boride. High resolution analyses coupled to selected area diffraction highlighted the nanostructure of the Zr_2Cu alloy, where possibly ZrB_2 reaction grains tended to anchor epitaxially to the pre-existing ZrB_2 lath, Fig. 8c,d. This microstructure assembly suggests that the phase transformation front moves quickly, leaving behind two solid products upon a rapid cooling of a eutectic system. Since the transition happens quickly and diffusion lengths are limited due to the low processing temperature of 1200°C, the atoms cannot move far to reach an equilibrium structure and result in fine lamellae by shortening the diffusion distance between the two solid phases.The grain boundaries of large ZrB_2 grains were often decorated with CuO phase, Fig. 9a, with which weak bonds were established owing to the poor wettability and the different coefficient of thermal expansion, reported even to be negative for CuO[39] and thus resulting in a predominant intergranular fracture of the matrix, Fig. 9b, possibly further contributing to additional toughening.

Regarding the residual Zr_2Cu melt phase, it was either found as irregularly shaped or as faceted crystals, Fig. 7e & g, respectively, possibly in relation to the Zr and B dissolved in it.

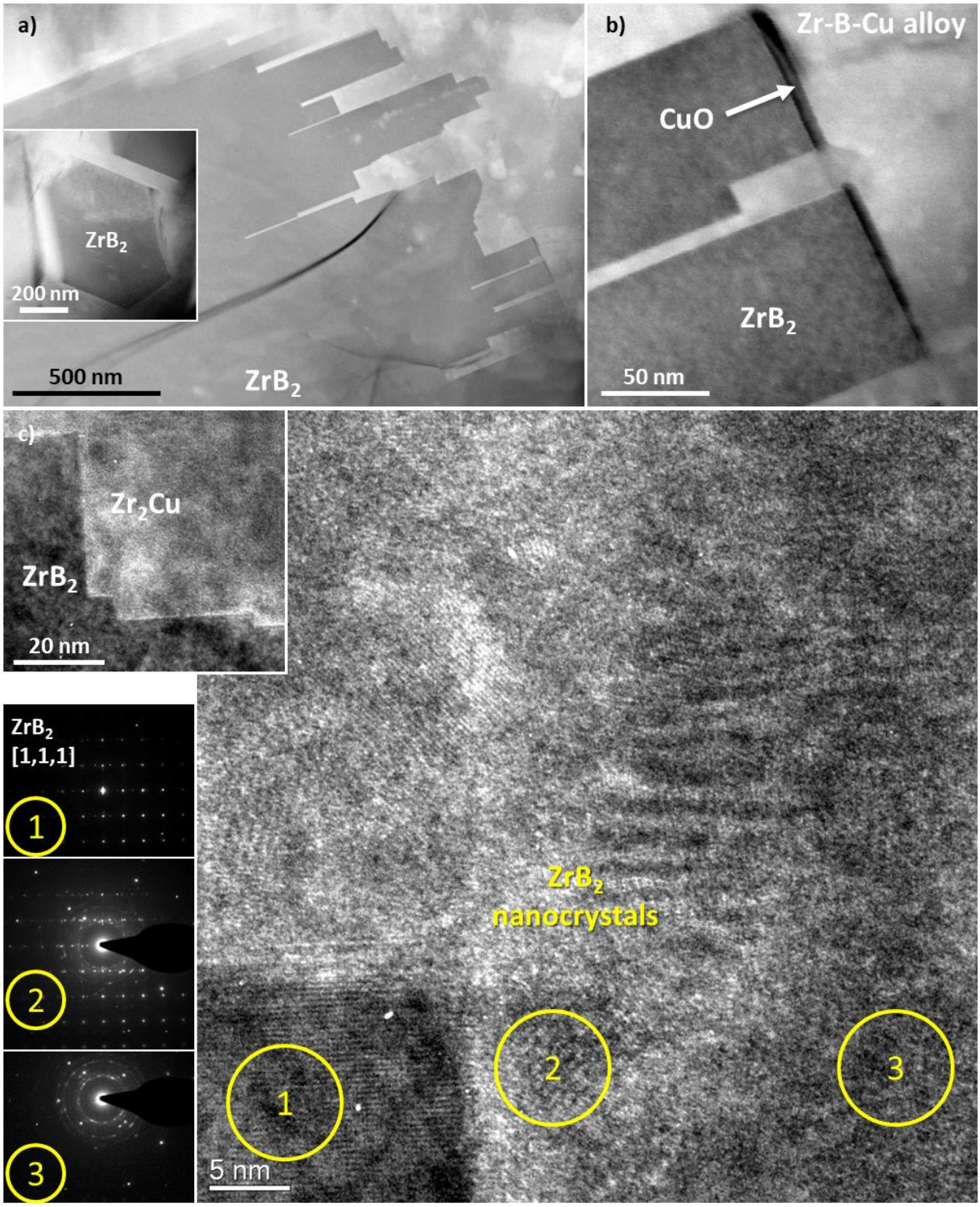

Figure 8. a) BF-TEM images of "lamellar eutectics" grains of ZrB_2 in material 2 showing b) CuO at the precipitation front and c) corresponding HR-TEM coupled with SAED recorded in different positions and showing the incipient formation of nanocrystals in the Zr-Cu-B alloy and anchorage to the growing ZrB_2 lath.

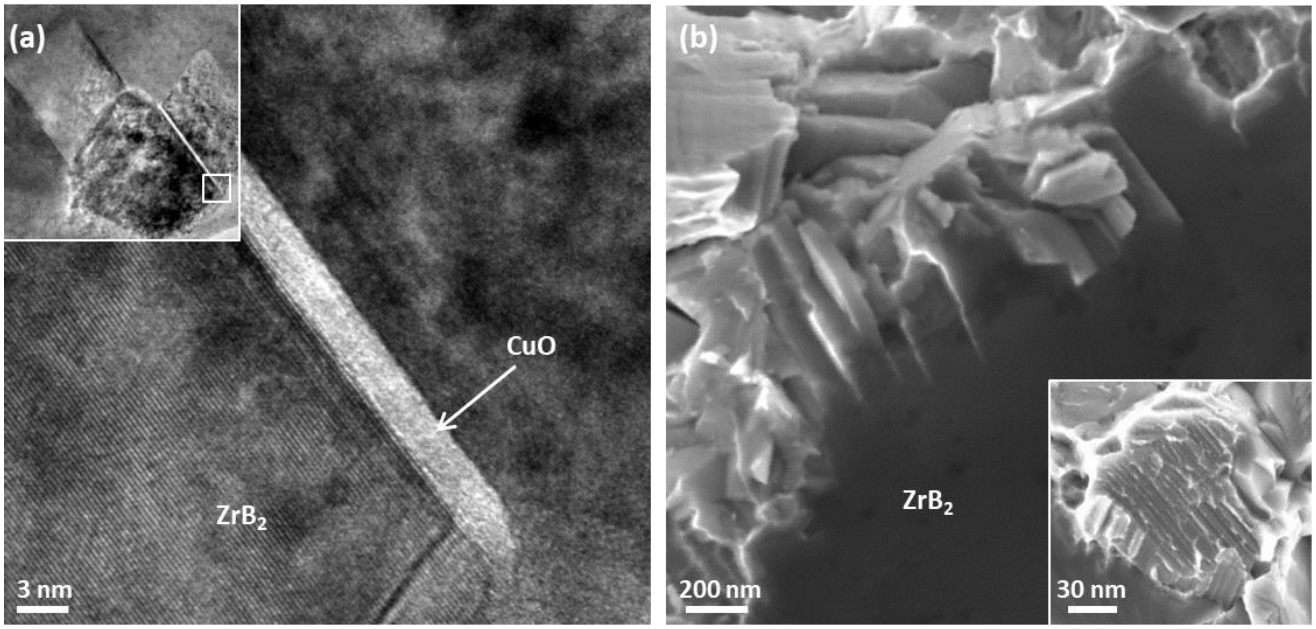

Figure 9. HR-TEM image of the RMI UHTCMC, material 2, showing ZrB_2 boundaries wetted by a CuO film resulting in weak bonds that promoted intergranular fracture of the matrix as displayed in b) where interlocking with metal phase on multiple scale-span is highlighted.

According to TEM investigations on the material 2, the microstructure of directionally solidified lamellar eutectics in ZrB_2 grains is the trace left behind in the solid by the periodic stationary pattern that the solid-liquid interface occurred during growth. Such growth pattern is the result of a dynamic balance between the competing diffusion in the liquid and capillary forces at the interface. [40]

As the Zr-Cu-B melt rich in Zr_2Cu crystallized, an excess of Zr-B remained and diffused a short distance laterally, due to the limited atoms mobility at such low temperatures,[41], [42] where it was incorporated in the ZrB_2. Similarly, the Zr-Cu atoms "rejected" ahead of the local melt phase diffused to the tips of the adjacent lamellae, resulting in stripes of the two crystals as shown in Fig. 8a. Such a structure defined as "lamellar eutectics" is energetically preferentially adopted in order to allow the phases to form but reduce the distance of diffusion. Therefore, the formation of such engrailed structure can be described as result of a dynamic process where the nucleation and growth of a new lath fragment is determined by continuous variations of the local super-saturation of the local melt and interdiffusion of Zr-Cu and Zr-B at the solidfication front, with the thickness of the lamella being controlled by the lateral diffusion velocity, as sketched in Fig. 10.

The degree of jagging and lath length were observed to decrease with the increase of B available in the melt,[32] suggesting that an increase of B amount in the melt leads to lower Zr-Cu super-saturation and lower lamella grow rate of both Zr_2Cu and ZrB_2 phases. For high local super-saturation, 2D nucleation is preferred over a homogeneous one from the point of view of achieving energetically stable interfaces.

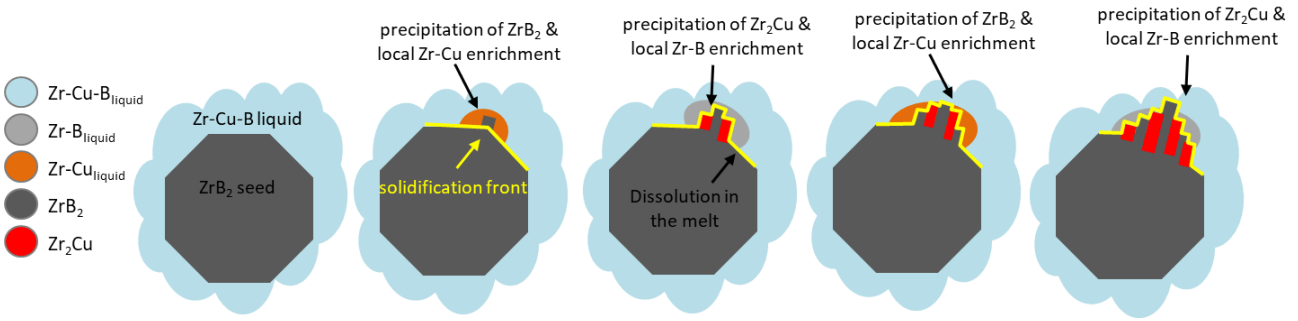

Fig. 10: Sketch of the formation of the lamellar eutectic structure on ZrB_2 seed. Local super-saturation of Zr-Cu or Zr-B and low atom mobility owing to the low temperature and rapid cooling process provoke the development of 2D laths of alternating composition.

The realization and microstructural analysis of material 2 evidenced that the reactive melting method is an effective technique to obtain almost fully dense refractory composites with microstructural features going from the micro- to the nano-sized scale length and therefore able to offer multiple synergistic reinforcing phenomena: from the carbon fiber pull-out to the crack deflection around 100-200 nm wide laths. However, it has to be remarked that the performance of such composites at high temperature are not expected to be relevant, owing to the residual amount of Cu-based low-melting compounds.

4. Conclusions

This work first explored the reactions occurring between a Zr_2Cu melting phase and possible compounds intended for use in ultra-refractory ceramic matrix composite, i.e. SiC, TiB_2 and ZrB_2.

Very good agreement, in terms of microstructure evolution, was assessed between sessile drop tests, singularly carried out on the three above substrates to obtain information on contact angle thereof and on the infiltration capability of the melt, in view of producing a multiphasic ultra-high temperature ceramic matrix composite by reactive melt infiltration (RMI), comprising a TiB_2-coated carbon fiber preform infiltrated with the Zr_2Cu at 1500°C. Main features of the composite were the precipitation of ZrB_2 and ZrC sub-micrometric faceted grains in the matrix and a general damage of both fiber and fiber coating, which were penetrated by the melt.

Subsequently, a second composite was prepared introducing additional ZrB_2-B that enabled to decrease the RMI process temperature down to 1200°C in an attempt to reduce the fiber damage degree during preparation, thus avoiding the need of using coated fibers, and reduce the processing costs. Despite this stratagem, these were notably altered by reaction with the Zr_2Cu melt and developed a ZrC crown around them, although pull-out was still promoted. In addition, the local B-rich environment provided the suitable conditions for the development of a dual-phase microstructure within the matrix composed of sub-micron-sized grains and of larger ZrB_2 grains, partially dissolved in the melt and re-precipitated assuming a lamellar eutectic structure. The lamellae, alternating ZrB_2 and Zr_2Cu phases had nano-sized dimensions and were well

interlocked. The simultaneous presence of microstructural features going from the micro- to the nano-sized scale length, i.e. from the carbon fiber pull-out, to the crack deflection around the 100-200 nm wide laths, is potentially able to offer multiple synergistic reinforcing phenomena and thus to be a valuable approach to develop materials for extreme environments.

Acknowledgements

The research leading to these results has received funding from the European Community's Seventh Framework Programme (FP7/2011-2014) under grant agreement No. 607182 (LIGHT-TPS) and from the European Union's Horizon 2020 "Research and innovation programme" under grant agreement No. 685594 (C3HARME). The authors would like to thank the colleagues from German Aerospace Center (DLR), Institute of Structures and Design, Department of Ceramic Composites and Structures, Stuttgart, Germany, for valuable discussion and use of laboratories. TEM analyses were conducted as a part of the Cooperative Agreement n. W911NF-19-2-0253 jointly sponsored by the U.S. Army DEVCOM and by the U.S. ONR. The views and conclusions contained in this document are those of the authors and should not be interpreted as representing the official policies, either expressed or implied, of the U.S. Army DEVCOM, U.S. ONR or the U.S Government.

References

[1] R. M. Sullivan, «A Model for the Oxidation of C/SiC Composite Structures», 216, 2003.

[2] D. Glass, «Ceramic Matrix Composite (CMC) Thermal Protection Systems (TPS) and Hot Structures for Hypersonic Vehicles», *15th AIAA International Space Planes and Hypersonic Systems and Technologies Conference*, March 2007, 1–36, 2008. doi: 10.2514/6.2008-2682.

[3] Y. Wang, Z. Chen, S. Yu, «Ablation behavior and mechanism analysis of C / SiC composites», *Journal of Materials Research and Technology*, 5 [2], 170–182, 2015. doi: 10.1016/j.jmrt.2015.10.004.

[4] L. Steg, H. Lew, «Hypersonic ablation», Chapter 32 in AGARDoraph vol.68, W.C. Nelson ed., pp. 629-680, 1964. doi.org/10.1016/B978-1-4831-9828-6.50037-0.

[5] T.H. Squire, J. Marschall, «Material property requirements for analysis and design of UHTC components in hypersonic applications», *Journal of the European Ceramic Society*, 30 [11] 2239–2251, 2010. doi: 10.1016/j.jeurceramsoc.2010.01.026.

[6] M.M. Opeka, I.G. Talmy, E.J. Wuchina, J.A. Zaykoski, S.J. Causey, «Mechanical, Thermal, and Oxidation Properties of Refractory Hafnium and zirconium Compounds», *Journal of the European Ceramic Society*, 19 [13-14], 2405–2414, 1999. doi: 10.1016/S0955-2219(99)00129-6.

[7] W.G. Fahrenholtz, E.J. Wuchina, W.E. Lee, Y.Zhou, *Ultra-High Temperature Ceramics: Materials for Extreme Environment Applications*. Hoboken, New Jersey: John Wiley & Sons Inc., 2014. doi: 10.1002/9781118700853.

[8] L.M. Rueschhoff, C.M. Carney, Z.D. Apostolov, M.K. Cinibulk, «Processing of fiber-reinforced ultra-high temperature ceramic composites: A review», *International Journal of Ceramic Engineering & Science*, 2, 22–37, 2020. doi: 10.1002/ces2.10033.

[9] A. Paul, D.D. Jayaseelan, S. Venugopal, E. Zapata-Solvas, J. Binner, B. Vaidhyanathan, A. Heaton, P. Brown, «UHTC-composites for hypersonic applications», *American Ceramic Society Bulletin*, 91 [1] 22, 2012. https://ceramics.org/wp-content/uploads/2012/01/janfeb12cover.pdf

[10] A. Paul, S. Venugopal, J.G. P. Binner, B. Vaidhyanathan, A.C. J. Heaton, P.M. Brown, «UHTC-carbon fibre composites: Preparation, oxyacetylene torch testing and characterisation», *Journal of the European Ceramic Society*, 33 [2] 423–432, 2013. doi: 10.1016/j.jeurceramsoc.2012.08.018.

[11] L. Silvestroni, D. Sciti, G.E. Hilmas, W.G. Fahrenholtz, J. Watts, « Effect of a weak fiber interface coating in ZrB_2 reinforced with long SiC fibers», Materials & Design, 88, 610-618, 2015. doi: 10.1016/j.matdes.2015.08.105

[12] S. Mungiguerra, G.D. Di Martino, A. Cecere, R. Savino, L. Zoli, L. Silvestroni, D. Sciti, « Ultra-high-temperature testing of sintered ZrB2-based ceramic composites in atmospheric re-entry environment», International Journal of Heat and Mass Tansfer, 156, 119910, 2020. doi: 10.1016/j.ijheatmasstransfer.2020.119910

[13] L. Silvestroni, E. Landi, K. Bejtka, A. Chiodoni, D. Sciti, «Oxidation behavior and kinetics of ZrB_2 containing SiC chopped fibers», Journal of the European Ceramic Society, 35 [16], 4377-4387, 2015. doi: 10.1016/j.jeurceramsoc.2015.07.024.

[14] J. Binner, M. Porter, B. Baker, J. Zou, V. Venkatachalam, V. Rubio Diaz, A. D'Angio, P. Ramanujam, T. Zhang, T.S.R.C. Murthy, «Selection, processing, properties and applications of ultra-high temperature ceramic matrix composites, UHTCMCs–a review», *International Materials Reviews*, 65 [7], 389–444, 2020. doi: 10.1080/09506608.2019.1652006.

[15] M. Kütemeyer, L. Schomer, T. Helmreich, S. Rosiwal, D. Koch, «Fabrication of ultra high temperature ceramic matrix composites using a reactive melt infiltration process», *Journal of the European Ceramic Society*, 36 [15], 3647–3655, 2016. doi: 10.1016/j.jeurceramsoc.2016.04.039.

[16] S. Tang, C. Hu, «Design, Preparation and Properties of Carbon Fiber Reinforced Ultra-High Temperature Ceramic Composites for Aerospace Applications: A Review», *Journal of Materials Science & Technology*, 33 [2], 117–130, 2016. doi: 10.1016/j.jmst.2016.08.004.

[17] J. Jiang, S. Wang, W. Li, Z. Chen, Y. Zhu, «Preparation of 3D C_f/ZrC–SiC composites by joint processes of PIP and RMI», *Materials Science and Engineering: A*, 607, 334–340, 2014. doi: 10.1016/J.MSEA.2014.03.071.

[18] D. Wang, S. Dong, H. Zhou, X. Zhang, Y. Ding, G. Zhu, «Fabrication and microstructure of 3D C_f /ZrC-SiC composites: Through RMI method with ZrO_2 powders as pore-making agent», *Ceramics International*, 42 [6], 6720–6727, 2015. doi: 10.1016/j.ceramint.2016.01.041.

[19] S. Chen, C. Zhang, Y. Zhang, H. Hu, «Preparation and properties of carbon fiber reinforced ZrC–ZrB_2 based composites via reactive melt infiltration», *Composites Part B: Engineering*, 60, 222–226, 2014. doi: 10.1016/J.COMPOSITESB.2013.12.067.

[20] B. Heidenreich, «Melt Infiltration Process», in *Ceramic Matrix Composites*, John Wiley & Sons, Ltd, 2008, pp. 113–139. doi: 10.1002/9783527622412.ch5.

[21] Y. Tong, S. Bai, X. Liang, Q.H. Qin, J. Zhai, «Reactive melt infiltration fabrication of C/C-SiC composite: Wetting and infiltration», *Ceramics International*, 42 [15], 17174–17178, 2016. doi: 10.1016/j.ceramint.2016.08.007.

[22] M. Naikade, A. Ortona, T. Graule, L. Weber, «Liquid metal infiltration of silicon based alloys into porous carbonaceous materials. Part I: Modelling of channel filling and reaction phase formation», *Journal of the European Ceramic Society*, 42 [5], 1971–1983, 2022. doi: 10.1016/j.jeurceramsoc.2021.12.068.

[23] M. Naikade, C. Hain, K. Kastelik, R. Brönnimann, G. Bianchi, A. Ortona, T. Graule and L. Weber, «Liquid metal infiltration of silicon based alloys into porous carbonaceous materials. Part II: Experimental verification of modelling approaches by infiltration of Si-Zr alloy into idealized microchannels», *Journal of the European Ceramic Society*, 42 [5], 1984–1994, 2022. doi: 10.1016/j.jeurceramsoc.2022.01.004.

[24] H.M. Chen, F. Zheng, H.S. Liu, L.B. Liu, Z.P. Jin, «Thermodynamic Assessment of B-Zr and Si-Zr Binary Systems», *Journal of Alloys and Compounds*, 468 [1–2], 209–216, 2009. doi: 10.1016/j.jallcom.2008.01.061

[25] H. Okamoto, «Cu-Zr (Copper-Zirconium)», *Journal of Phase Equilibria and Diffusion*, 33 [5], 417–418, 2012. doi: 10.1007/s11669-012-0077-1.

[26] S. Zhang, S. Wang, W. Li, Y. Zhu, Z. Chen, «Preparation of ZrB_2 based composites by reactive melt infiltration at relative low temperature», *Materials Letters*, 65 [19–20], 2910–2912, 2011. doi: 10.1016/j.matlet.2011.06.070.

[27] M.L. Muolo, E. Ferrera, R. Novakovic, A. Passerone, «Wettability of zirconium diboride ceramics by Ag, Cu and their alloys with Zr», *Scripta Materialia*, 48 [2], 191–196, 2003. doi: 10.1016/S1359-6462(02)00361-5.

[28] M. Kütemeyer, T. Helmreich, S. Rosiwal, D. Koch, «Influence of zirconium-based alloys on manufacturing and mechanical properties of ultra high temperature ceramic matrix composites», *Advances in Applied Ceramics*, 117 [1], s62–s69, 2018. doi: 10.1080/17436753.2018.1509810.

[29] M. Kütemeyer, «Development of Ultra High Temperature Matrix Composites using a Reactive Melt Infiltration Process», Fakultät für Maschinenbau (MACH), 2021. https://publikationen.bibliothek.kit.edu/1000130618.

[30] M. Kütemeyer, D. Shandler, D. Koch, M. Friess, «Reactive melt infiltration of boron containing fiber reinforced preforms forming a ZrB_2 matrix», in *Processing and Properties of Advanced Ceramics and Composites VII: Ceramic Transactions*, 252, pp. 169–180, 2015. doi: 10.1002/9781119183860.ch18.

[31] D. Sciti, S. Guicciardi, L. Silvestroni, «SiC chopped fibers reinforced ZrB_2: Effect of the sintering aid», *Scripta Materialia*, 64 [8], 769–772, 2011. doi: 10.1016/j.scriptamat.2010.12.044.

[32] A. Vinci, L. Zoli, P. Galizia, M. Kütemeyer, D. Koch, M. Frieß, D. Sciti, «Reactive melt infiltration of carbon fibre reinforced ZrB_2/B composites with Zr_2Cu», *Composites Part A: Applied Science and Manufacturing*, 137, 105973, 2020. doi: 10.1016/j.compositesa.2020.105973.

[33] M. Xu, Y.Y. Ye, J.R. Morris, D.J. Sordelet, M.J. Kramer, «In situ observation of thermal expansion of tetragonal C11b phase in $Zr_2Cu_{(1-x)}Pd_x$ alloys», *Intermetallics*, 18 [1], 8–13, 2010. doi: 10.1016/j.intermet.2009.05.016.

[34] J. García, V. Collado Ciprés, A. Blomqvist, B. Kaplan, «Cemented carbide microstructures: a review», *International Journal of Refractory Metals and Hard Materials*, 80, 40–68, 2019. doi: 10.1016/j.ijrmhm.2018.12.004.

[35] S. Guo, «Densification, microstructure, elastic and mechanical properties of reactive hot-pressed ZrB_2–ZrC–Zr cermets», *Journal of the European Ceramic Society*, 34 [3], 621–632, 2014. doi: 10.1016/j.jeurceramsoc.2013.09.002.

[36] M. Tarraste, K. Juhani, J. Pirso, M. Viljus, «Reactive Sintering of Bimodal WC-Co Hardmetals», *Materials Science (Medziagotyra)*, 21 [3], 2015. doi: https://doi.org/10.5755/j01.ms.21.3.7511.

[37] I. Engström, B. Lönnberg, «Thermal expansion studies of the group IV-VII transition-metal disilicides», *Journal of Applied Physics*, 63 [9], 4476–4484, 1988. doi: 10.1063/1.340168.

[38] D.A. Porter, K.E. Easterling, M.Y. Sherif, «Phase transformations», in *Metals and Alloys*, New York: CRC Press, 1992, p. 222.

[39] L.A. Neely, E.M. See, H.D. Robinson, V. Kochergin, «Thermal expansion of Cu(II)O nano- and micro-particles and composites at cryogenic temperatures», *Basic Solid State Physics*, 249 [9], 1698–1703, 2012. doi: 10.1002/pssb.201248121.

[40] M. Tarraste, K. Juhani, J. Pirso, M. Viljus, «Reactive Sintering of Bimodal WC-Co Hardmetals», *Materials Science (Medziagotyra)*, 21 [3], 2015. doi: 10.5755/j01.ms.21.3.7511.

[41] H. Hofmann, G. Petzow, «Structure and properties of reaction hot-pressed B_4C-TiB_2-W_2B_5 materials», *Journal of The Less-Common Metals*, 117 [1–2], 121-127, 1986. doi: 10.1016/0022-5088(86)90020-2.

[42] X. Zheng, P. Shen, X. Han, Q. Lin, F. Qiu, Y. Zhang, Q. Jiang, «Wettability and reactivity between B_4C and molten $Zr_{55}Cu_{30}Al_{10}Ni_5$ metallic glass alloy», *Materials Chemistry and Physics*, 117 [2], 377–383, 2009, doi: 10.1016/j.matchemphys.2009.06.017.